

Tunable Plasmonic Filter Based on Graphene Split-Ring

Yixiao Gao^{1,2} · Guobin Ren^{1,2} · Bofeng Zhu^{1,2} · Lin Huang^{1,2} ·
Haisu Li^{1,2} · Bin Yin^{1,2} · Shuisheng Jian^{1,2}

Received: 27 May 2015 / Accepted: 4 August 2015 / Published online: 14 August 2015
© Springer Science+Business Media New York 2015

Abstract We propose in this paper a tunable plasmonic filter based on graphene split-ring (GSR) resonator. It is found the resonances could be classified into two categories, i.e., even-parity and odd-parity mode according to the symmetry of field profile in GSR. The coupling between graphene nanoribbon and GSR is GSR-orientation sensitive, and the odd-parity mode presents a greater sensitivity due to its asymmetric field profile. The transmission spectrum of the proposed filter could be efficiently modified by tuning the shape, orientation, and Fermi level of GSR. The proposed structure can be applied in the tunable ultra-compact graphene plasmonic devices for future nanoplasmonic applications.

Keywords Graphene plasmons · Split-ring resonator · Plasmonic filter

Introduction

Surface plasmons (SPs), electromagnetic waves couple to free-electron excitations at the surface of a conductor, have attracted increasing research interest in past decades [1] because it provides the possibility to route and manipulate light waves at the subwavelength scale which is highly needed by the nanophotonic technologies. Graphene, a one-atom-thick

carbon layer, has been predicted and demonstrated to sustaining SPs in infrared to terahertz frequencies [2]. Graphene plasmons (GPs) have many appealing properties such as extreme confinement, tunability by gating or doping, and low Ohmic losses, rendering graphene as a promising platform to build highly integrated active plasmonic devices. Many tunable devices were proposed based on GPs, such as modulator [3], plasmonic filters [4–6], logic gates [7], and optical antennas [8].

Graphene nanoribbon (GNR) could be applied for efficient GP waveguiding with small mode size and high mode index [9]. Despite the large wavevector mismatch between GPs and free-space photons, several methods have been devised to excite GPs efficiently, such as grating coupling [10, 11] and tapered polaritonic slab waveguide [12]. By using randomly stacked multilayer graphene, the wavevector of GPs can be substantially reduced as well [13, 14]. Resonator-waveguide-coupled system is a generic configuration in photonics devices which is widely used in the field of filtering, switching, and sensing. Recently, numerous studies have been taken out to investigate the graphene-based plasmonic resonators, such as graphene ring [6], graphene disk [5], and graphene resonant ribbon [15]. The resonator has a strong impact on the transmission and reflection characteristics of the GNR plasmonic waveguide, and different configurations of resonator have distinct properties.

Split-ring resonator is a fundamental element in the metamaterials field and also known as “meta-molecule.” Graphene split-ring (GSR) resonator shows a stronger magnetic response than its metallic counterpart in infrared to terahertz frequencies [16]. In this paper, we propose a plasmonic filter consisting of a GNR side coupled by a GSR, which could be realized on monolayer graphene by applying different bias voltages to different regions. The proposed structure is numerically investigated by 3D finite element method (FEM). We first compare the transmission spectra of GNRs side coupled

✉ Guobin Ren
gbren@bjtu.edu.cn

¹ Key Lab of All Optical Network and Advanced Telecommunication Network of EMC, Beijing Jiaotong University, Beijing 100044, China

² Institute of Lightwave Technology, Beijing Jiaotong University, Beijing 100044, China

by graphene ring and by GSR and define two kinds of resonant modes in GSR according to the symmetry of field profile in GSR. Next, we investigate the influence of the effective cavity length, the orientation of GSR, and the distance between GSR and GNR on the resonant wavelength and resonance strength, and reveal that the GSR-GNR plasmonic coupling is dependent on the orientation of GSR and the odd-parity mode is found to be more sensitive to the orientation due to the asymmetric field profile. Finally, we study the tunability of the proposed filter by varying the Fermi level of graphene. The proposed plasmonic filter is electrically tunable and ultra-compact in size, and our study may provide an alternative way for designing GP-based devices.

Structure and Simulation Method

Figure 1 shows the schematic diagram of the proposed plasmonic filter. GSR is realized by introducing a split on a graphene ring with outer radius R and width W_R . The split width corresponds to a sector angle θ , as denoted in Fig. 1. The orientation of GSR is measured by the angle ϕ between the center of the gap and x axis. The width of graphene ribbon is $W=50$ nm. GP modes on GNR were characterized by the node number of the mode profiles [17], and we only consider the fundamental mode (i.e., the even-parity edge mode depicted in the inset of Fig. 1) as the input due to its strong interaction with GSR [6]. Single mode operation in GNR can be realized by reducing the ribbon width W or increasing the Fermi energy of graphene [9]. Without loss of generality, we consider the whole structure is embedded in air.

The electromagnetic property of graphene can be characterized by its dynamic conductivity σ , which is related to temperature, Fermi energy E_f , scattering time τ , and electromagnetic frequency ω . Both interband and intraband transition of electrons in graphene contribute to σ . In the infrared to terahertz frequencies, the interband transition could be

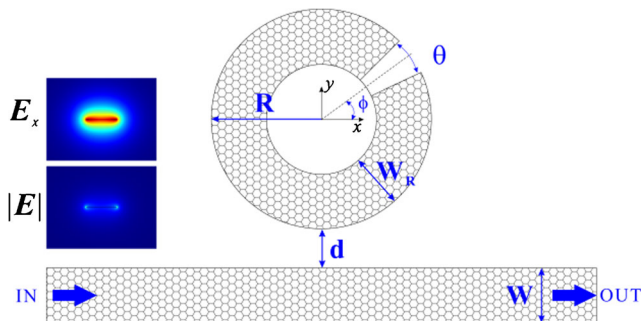


Fig. 1 Schematic of the proposed filter consisting of a GNR with width W and a GSR with outer radius R , width W_R , and split width corresponding to a sector angle θ . The orientation of GSR is denoted by ϕ as indicated in figure. The distance between GSR and ribbon is d . The insets show the x component (E_x) and normalized ($|E|$) electric field of edge mode on GNR

neglected, and we only need to consider the intraband transition. σ can be well described by Drude model [16, 18],

$$\sigma = \frac{ie^2}{\pi\hbar^2} \frac{E_f}{(\omega + 1/\tau)} \quad (1)$$

where e is electron charge and \hbar is the reduced Planck's constant. In the 3D FEM simulation, graphene is modeled as a thin layer with thickness $t=1$ nm and with effective permittivity $\epsilon_{\text{eq}}=1+i\sigma/\omega\epsilon_0t$ [17], and scattering time τ is 0.5 ps based on recent graphene plasmonic studies [12]. As depicted in Fig. 1, the GP mode is injected at the “IN” port. Numerical calculation of input mode is implemented on the IN port face, and only fundamental mode is excited due to the single mode GNR we choose. The “OUT” port absorbs the outgoing energy in the excited modes.

Result and Discussions

Figure 2a shows comparison of the transmission spectra of the filter structures based on side-coupled GSR and graphene ring resonators. The radius and width of both resonators are 100 and 50 nm. The distance between resonator and ribbon is 20 nm. The split width θ and orientation ϕ of GSR are 10 and 90 deg, respectively. The Fermi level of graphene is

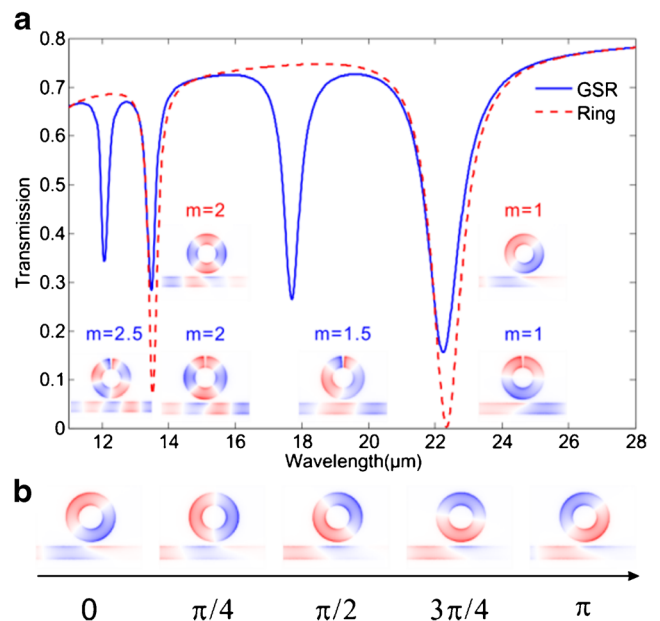
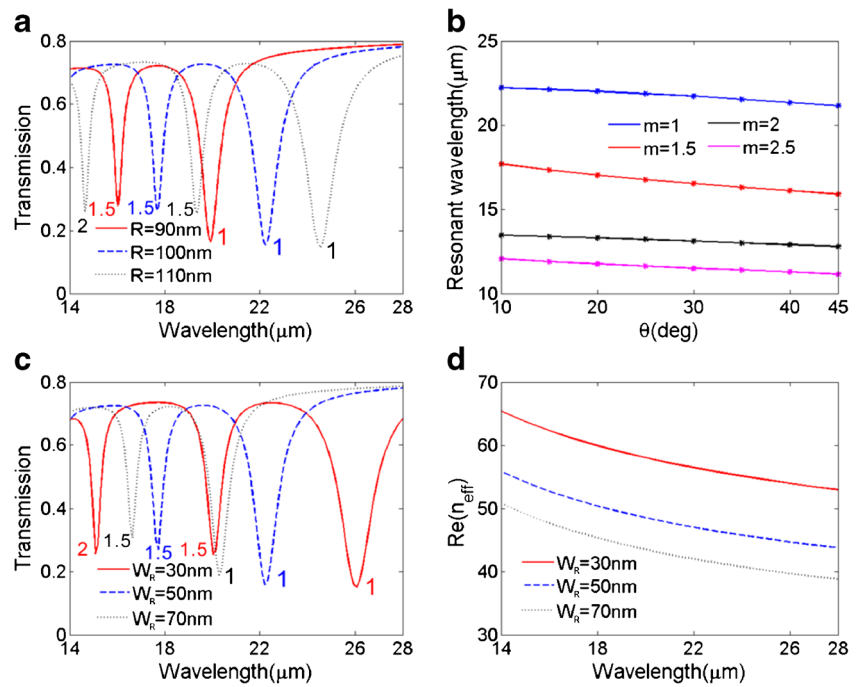


Fig. 2 **a** Comparison of the transmission spectra of side-coupled GSR and graphene ring filters. $R=100$ nm, $W_R=50$ nm, $d=20$ nm, $E_f=0.2$ eV, for both GSR and graphene ring, $\theta=10$ deg and $\phi=90$ deg for GSR. m denotes the order of resonance and the corresponding field profiles are depicted in the insets. The field profiles are snapshots of the electric fields E_z at 3 nm above the graphene. **b** Field profiles of graphene ring resonator in half an optical period at $m=1$ resonance, frequency $f=50$ THz, nanowire radius $R=120$ nm, distance $d=50$ nm, and chemical potential $\mu_c=0.6$ eV

Fig. 3 **a** Transmission spectra of the side-coupled GSR filter with different R . **b** The resonant wavelengths as a function of GSR split width θ . **c** Transmission spectra of the side-coupled GSR filter with different W_R . **d** Mode index of fundamental mode in GNR with different width. The parameters of the filter are set as Fig. 2 unless they are changed for comparison. The numbers in the figure indicate the order of resonance



$E_f=0.2$ eV. As for the graphene ring (red dashed curve), two transmission dips emerge at $\lambda=22.34$ and 13.52 μm . Figure 2b shows the field profiles at the resonance with $\lambda=22.34$ μm in the graphene ring at different phases in half an optical period. We can see that the resonant mode circulates in the ring, indicating the fact that the resonant mode in graphene ring is travelling wave mode [19]. The GSR is formed by introducing a split ($\theta=10$ deg, $\phi=90$ deg) in the graphene ring, and a slight blue-shift of the original resonant wavelength can be observed ($\lambda=22.24$ μm , 13.48 μm). New transmission dips appear at $\lambda=17.70$ and 12.07 μm . The

resonant modes in GSR are obviously standing wave modes [19] due to the introduced split.

The field profiles in graphene ring and GSR at corresponding resonant wavelengths are depicted in the insets of Fig. 2a. The resonance modes in GSR could be categorized into two kinds according to the field profile symmetry. Even-parity modes are at $\lambda=22.24$ and 13.48 μm , and odd-parity modes are at $\lambda=17.70$ and 12.07 μm . The resonant wavelength of GSR could be obtained by the Fabry-Perot (F-P) model. The effective F-P cavity length $L_{\text{eff}}=(1-\theta/360^\circ)2\pi R_{\text{eff}}$, where $R_{\text{eff}}=R-W_R/2$ and θ is in the

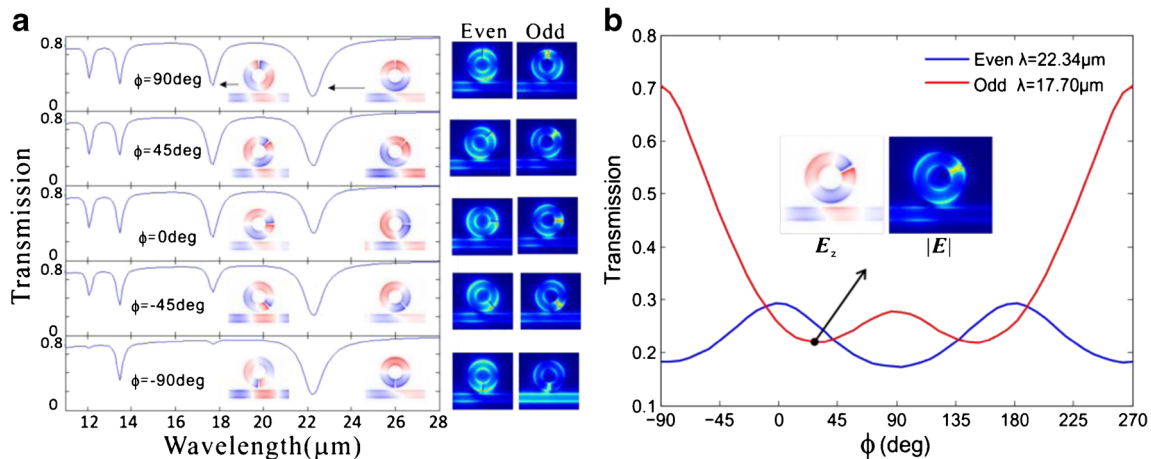


Fig. 4 **a** Transmission spectra of the side-coupled GSR filter with different ϕ . *Insets* show the E_z profiles at the first two resonances, and the corresponding $|E|$ profiles are shown in the *right column*. **b** The

minimum transmission ratio at the $m=1$ and $m=1.5$ resonances as a function of GSR orientation ϕ . The *inset* shows the field profile of odd-parity mode with the lowest transmission ratio ($\phi=27.5$ deg)

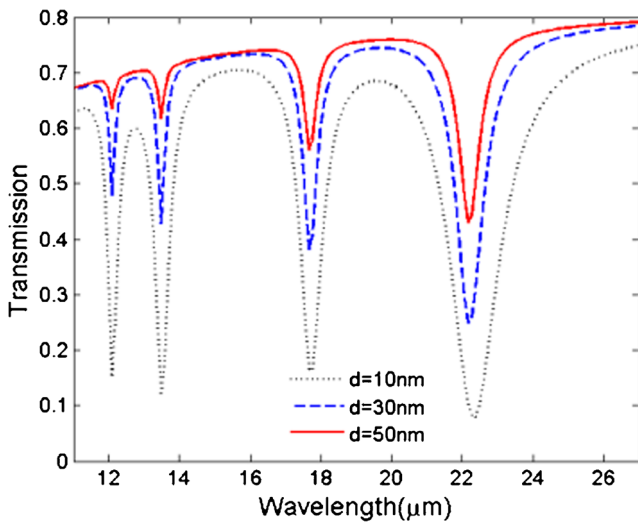


Fig. 5 Transmission spectra of the side-coupled GSR filter with different GSR-GNR distance d . Other parameters of the filter are set as Fig. 2

unit of degree. In order to achieve the standing wave condition, the resonant wavelength λ_m has to satisfy the following equation,

$$\lambda_m = \frac{n_{\text{eff}} L_{\text{eff}}}{m + \phi_r / \pi} \quad (2)$$

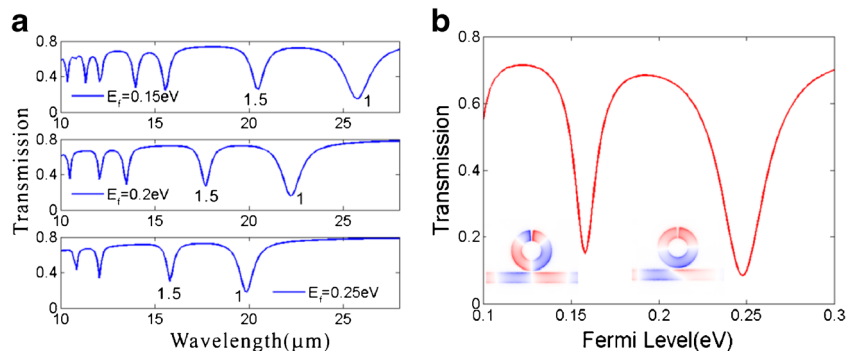
where n_{eff} is the effective mode index of GSR and ϕ_r is the phase shift of GPs reflected at either edge of the split in GSR. m can be regarded as the order of resonance. For even-parity modes, $m=1, 2, 3, \dots$, whereas for odd-parity modes, $m=1.5, 2.5, 3.5, \dots$

The effective F-P cavity length L_{eff} is jointly determined by split width θ , outer radius R , and width W_R of GSR. Next, we investigate the influence of these parameters on the transmission characteristics of proposed filter. The parameters of the filter (i.e., W_R, R, d, θ , and ϕ) are set as Fig. 2 unless they are changed for comparison. Figure 3a shows the transmission spectra of the proposed filter with different R . The whole spectra tend to red shift with the radius increasing. The θ -dependent resonant wavelengths of the first four order resonances are depicted in Fig. 3b. The resonant wavelength is

linearly decreased with θ increasing. This is because split width θ and radius of GSR are both linearly related with L_{eff} , leading to the linear shift of the resonant wavelength. However, it can be observed that the resonant wavelength of odd-parity resonances is more sensitive to the change of split width. For example, when θ varies from 10 to 45 deg, the resonant wavelengths of $m=1$ and 1.5 modes change by 1.07 and 1.8 μm , respectively. Figure 3c shows the W_R -dependent transmission spectra with L_{eff} and d kept unchanged. The resonant wavelengths of the same order tend to red shift as W decreases, which results from the W_R -dependent n_{eff} in GSR. The n_{eff} can be approximated by the mode index of fundamental mode in GNR with the same width. Figure 3d depicts the mode index of GNR with a width of 30, 50, and 70 nm. GNR with a narrower width has a larger mode index, leading to an increase of resonant wavelength in order to satisfy the standing wave condition (see Eq. 2).

As discussed above, the resonant wavelengths are affected by the effective cavity length and the mode index of GSR. The GSR orientation ϕ is also expected to influence the resonances. The transmission ratio at the resonant wavelength represents resonance strength, i.e., a lower (higher) transmission ratio suggests stronger (weaker) resonance strength. Figure 4a shows the transmission spectra of the proposed filter with different GSR orientations ϕ , and other parameters R, W, θ, d , and E_f are set the same as Fig. 2. The resonant wavelength is determined by the standing wave condition Eq. (2). Therefore, the positions of transmission dips are independent on the GSR orientation ϕ as depicted in Fig. 4a. However, the minimum transmission at each resonant wavelength, i.e., the resonance strength, is influenced by the GSR orientation, especially for the odd-parity mode. For example, at $\lambda=17.70 \mu\text{m}$ (odd-parity mode), when $\phi=90, 45, 0, -45$, and -90 deg, the transmission ratio are 0.27, 0.22, 0.24, 0.45, and 0.70, respectively. As for the even-parity resonance, the resonance strength has a weaker dependence on the GSR orientation. Figure 4b shows the transmission ratio at the $m=1$ ($\lambda=22.24 \mu\text{m}$) and $m=1.5$ ($\lambda=17.70 \mu\text{m}$) resonances with GSR orientation ϕ varying from -90 to 270 deg in a counter-clockwise direction. Both curves for even and odd-parity modes are symmetrical about

Fig. 6 a Transmission spectra of the proposed filter with different GSR Fermi levels. **b** Transmission ratio as a function of Fermi level at the wavelength 20 μm . Insets show the field profiles when $E_f=0.158$ and 0.247 eV



$\phi=90$ deg, i.e., the same resonance strength can be observed when GSR is oriented symmetrically about y axis, which indicates the fact that same transmission ratio could be obtained when field is injected from either port of the proposed filter with a fixed GSR orientation (see Fig. 2). The transmission ratio of odd-parity mode varies from 0.21 to 0.71 with GSR rotating, and that of the even-parity mode varies from 0.29 to 0.17. The lowest transmission ratio of even-parity mode occurs at $\phi=-90$ and 90 deg, and the highest one is at $\phi=0$ deg, whereas the lowest transmission ratio of odd-parity mode occurs at $\phi=27.5$ deg and the highest one is at $\phi=-90$ deg. The field of resonance in GSR forms standing wave pattern which rotates with different GSR orientation, as depicted in the insets of Fig. 4. Therefore, when the crest of standing wave in GSR is close to the GNR, the resonance in GSR is enhanced due to constructive interference between GSR and GNR. On the contrary, when the trough of standing wave is close to GNR, the resonance is weakened when field minimum of the standing wave is close to GNR because the fields in GSR and GNR oscillate out-of-phase.

The resonance strength in GSR is also influenced by the distance between GSR and graphene ribbon d . Figure 5 shows the transmission spectra of the proposed structure with d varying from 10 to 50 nm. The minimum transmission ratio at each resonance is increased with d increasing, which is a common phenomenon in resonator-waveguide-coupled system. A reducing resonance strength at shorter wavelengths could be observed, and a similar trend could be observed in Figs. 3 and 4. This is because field is tightly confined near the graphene structure at short wavelength range which deteriorates the coupling between GSR and ribbon.

Due to the unique properties of graphene, the transmission spectra of the proposed filter can be tuned by changing the Fermi level of graphene, which can be realized by electrical gating. Since the filtering characteristics mainly depends on the resonator, we change the Fermi level of GSR to examine the tunability of the proposed filter, while the Fermi level of ribbon is kept at 0.2 eV and other parameters are the same as Fig. 2. Figure 6a shows the transmission spectra with Fermi level of GSR set as 0.15, 0.2, and 0.25 eV. The resonant wavelength exhibit blue shift with Fermi level increasing, for example, when E_f is tuned from 0.15 to 0.25 eV, the resonant wavelength for $m=1$ resonance is changed from 25.70 to 19.91 μm . The transmission property at certain wavelength could be modified dramatically by a slight change of E_f . Figure 6b depicts the E_f -dependent transmission ratio at the wavelength of 20 μm . When E_f changes from 0.189 to 0.248 eV, the transmission ratio reduces from 0.68 to 0.08. The resonance type could also be tuned by varying E_f . The resonance in GSR at $E_f=0.247$ eV corresponds to even-parity modes, and at $E_f=0.158$ eV, the resonance becomes an odd-parity one (see the insets of Fig. 6b).

Conclusions

In summary, a tunable plasmonic filter consisting of a GSR resonator side coupled with a GNR is proposed and numerically analyzed by FEM method. The simulation result shows the resonances in GSR resonator has even- or odd-parity field profile, and the resonant wavelength can be predicted by using F-P model with integer or non-integer number indicating the mode order. The resonance strength is sensitive to the GSR orientation and the strength of odd-parity resonance shows a stronger dependence on due to its asymmetric field profile in GSR. The transmission spectra of the proposed filter can be changed by altering the split width, width, or outer radius of GSR, and the strength of resonance is inversely related to the distance between GSR and graphene ribbon. By increasing the Fermi level of GSR, the resonant wavelength tends to blue shift, and the even-parity resonance could be turned into odd-parity mode by properly changing the Fermi level. The proposed GSR side-coupled graphene ribbon structure offers the flexibility to tailor the transmission spectrum by carefully designing the GSR parameters and could be utilized to realize tunable compact graphene plasmon devices for future optical communication and processing in the mid-infrared frequencies.

Acknowledgments This work was supported by the Fundamental Research Funds for the Central Universities (no. 2015YJS018).

References

- Gramotnev DK, Bozhevolnyi SI (2010) Plasmonics beyond the diffraction limit. *Nat Photonics* 4(2):83–91. doi:10.1038/nphoton.2009.282
- Grigorenko AN, Polini M, Novoselov KS (2012) Graphene plasmonics. *Nat Photonics* 6(11):749–758. doi:10.1038/nphoton.2012.262
- Sensale-Rodriguez B, Yan R, Zhu M, Jena D, Liu L, Grace Xing H (2012) Efficient terahertz electro-absorption modulation employing graphene plasmonic structures. *Appl Phys Lett* 101(26):261115. doi:10.1063/1.4773374
- Tao J, Yu X, Hu B, Dubrovkin A, Wang QJ (2014) Graphene-based tunable plasmonic Bragg reflector with a broad bandwidth. *Opt Lett* 39(2):271. doi:10.1364/ol.39.000271
- Zhang L, Yang J, Fu X, Zhang M (2013) Graphene disk as an ultra compact ring resonator based on edge propagating plasmons. *Appl Phys Lett* 103(16):163114. doi:10.1063/1.4826515
- Li H-J, Wang L-L, Liu J-Q, Huang Z-R, Sun B, Zhai X (2013) Investigation of the graphene based planar plasmonic filters. *Appl Phys Lett* 103(21):211104. doi:10.1063/1.4831741
- Ooi KJ, Chu HS, Bai P, Ang LK (2014) Electro-optical graphene plasmonic logic gates. *Opt Lett* 39(6):1629–1632. doi:10.1364/OL.39.001629
- Liu P, Cai W, Wang L, Zhang X, Xu J (2012) Tunable terahertz optical antennas based on graphene ring structures. *Appl Phys Lett* 100(15):153111. doi:10.1063/1.3702819
- He S, Zhang X, He Y (2013) Graphene nano-ribbon waveguides of record-small mode area and ultra-high effective refractive indices

- for future VLSI. *Opt Express* 21(25):30664. doi:10.1364/oe.21.030664
10. Ju L, Geng B, Horng J, Girit C, Martin M, Hao Z, Bechtel HA, Liang X, Zettl A, Shen YR, Wang F (2011) Graphene plasmonics for tunable terahertz metamaterials. *Nat Nanotechnol* 6(10):630–634. doi:10.1038/nnano.2011.146
 11. Gao W, Shu J, Qiu C, Xu Q (2012) Excitation of plasmonic waves in graphene by guided-mode resonances. *ACS Nano* 6(9):7806–7813. doi:10.1021/nn301888e
 12. Nikitin AY, Alonso-Gonzalez P, Hillenbrand R (2014) Efficient coupling of light to graphene plasmons by compressing surface polaritons with tapered bulk materials. *Nano Lett* 14(5):2896–2901. doi:10.1021/nl500943r
 13. Smirnova DA, Shadrivov IV, Miroshnichenko AE, Smirnov AI, Kivshar YS (2014) Second-harmonic generation by a graphene nanoparticle. *Phys Rev B* 90(3). doi:10.1103/PhysRevB.90.035412
 14. Zhou X, Zhang T, Chen L, Hong W, Li X (2014) A graphene-based hybrid plasmonic waveguide with ultra-deep subwavelength confinement. *J Lightwave Technol* 32(21):3597–3601. doi:10.1109/jlt.2014.2350487
 15. Zhuang H, Kong F, Li K, Sheng S (2015) Plasmonic bandpass filter based on graphene nanoribbon. *Appl Opt* 54(10):2558. doi:10.1364/ao.54.002558
 16. Papasimakis N, Thongrattanasiri S, Zheludev NI, García de Abajo FJ (2013) The magnetic response of graphene split-ring metamaterials. *Sci Appl* 2(7), e78. doi:10.1038/lsa.2013.34
 17. Christensen J, Manjavacas A, Thongrattanasiri S, Koppens FH, de Abajo FJ (2012) Graphene plasmon waveguiding and hybridization in individual and paired nanoribbons. *ACS Nano* 6(1):431–440. doi:10.1021/nn2037626
 18. Fang Z, Thongrattanasiri S, Schlather A, Liu Z, Ma L, Wang Y, Ajayan PM, Nordlander P, Halas NJ, Garcia de Abajo FJ (2013) Gated tunability and hybridization of localized plasmons in nanostructured graphene. *ACS Nano* 7(3):2388–2395. doi:10.1021/nn3055835
 19. Li Q, Wang T, Su Y, Yan M, Qiu M (2010) Coupled mode theory analysis of mode-splitting in coupled cavity system. *Opt Express* 18(8):8367–8382. doi:10.1364/OE.18.008367